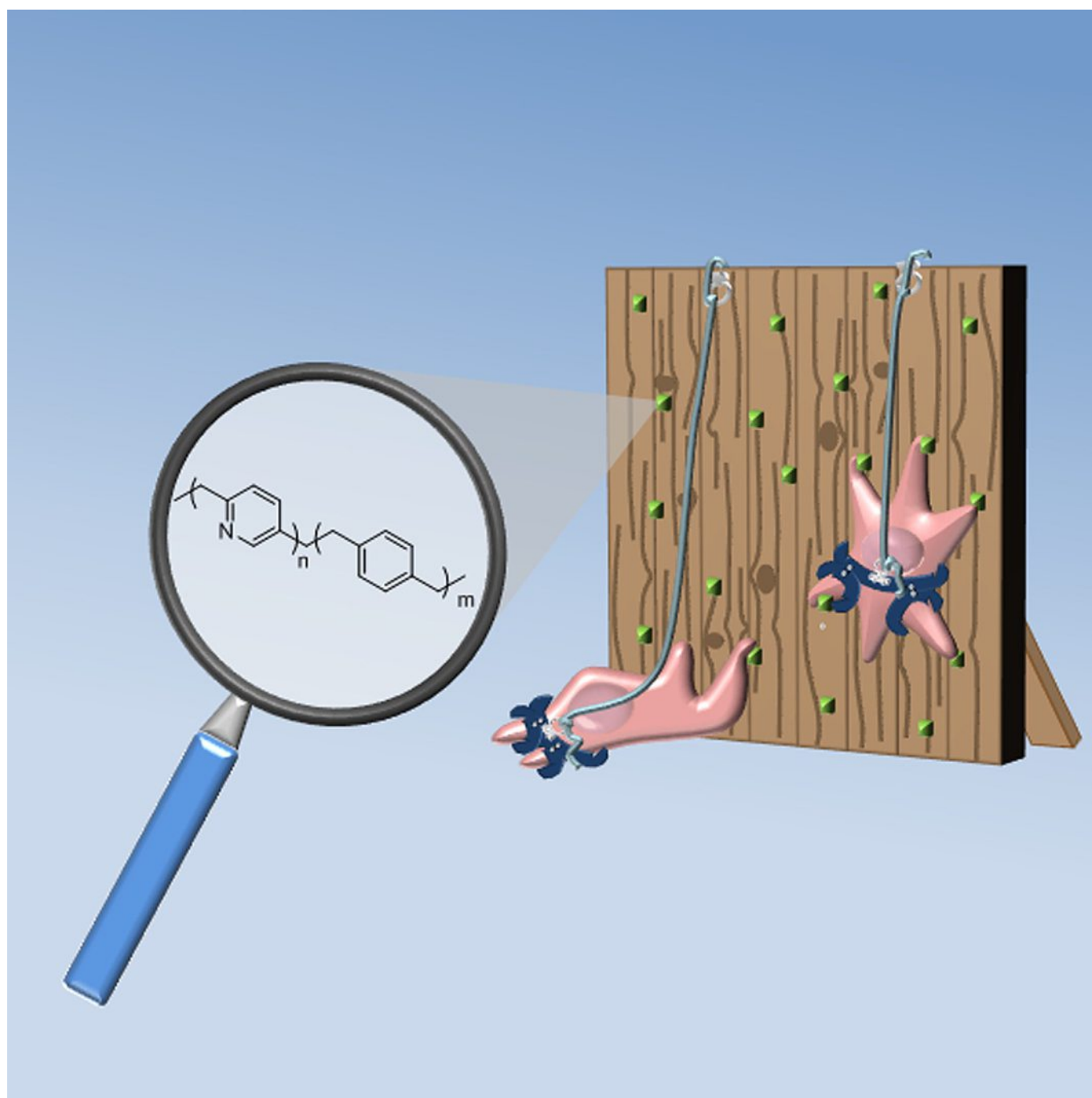


■ Chemical Vapor Deposition

Polylutidines: Multifunctional Surfaces through Vapor-Based Polymerization of Substituted Pyridinophanes

Florence Bally-Le Gall^{+, [a, b]} Christoph Hussal^{+, [a]} Joshua Kramer,^[c] Kenneth Cheng,^[d] Ramya Kumar,^[d] Thomas Eyster,^[d] Amy Baek,^[d] Vanessa Trouillet,^[e] Martin Nieger,^[f] Stefan Bräse,^{*, [c, g]} and Joerg Lahann^{*, [a, d]}



Abstract: We report a new class of functionalized polylutidine polymers that are prepared by chemical vapor deposition polymerization of substituted [2](1,4)benzo[2](2,5)pyridinophanes. To prepare sufficient amounts of monomer for CVD polymerization, a new synthesis route for ethynylpyridinophane has been developed in three steps with an overall yield of 59%. Subsequent CVD polymerization yielded well-defined films of poly(2,5-lutidinylene-co-*p*-xylylene) and poly(4-ethynyl-2,5-lutidinylene-co-*p*-xylylene). All polymers were characterized by infrared reflection-absorption spectroscopy, ellipsometry, contact angle studies, and X-ray photoelectron spectroscopy. Moreover, ζ -potential measurements revealed that polylutidine films have higher isoelectric points than the corresponding poly-xylylene surfaces owing

to the nitrogen atoms in the polymer backbone. The availability of reactive alkyne groups on the surface of poly(4-ethynyl-2,5-lutidinylene-co-*p*-xylylene) coatings was confirmed by spatially controlled surface modification by means of Huisgen 1,3-dipolar cycloaddition. Compared to the more hydrophobic poly-*p*-xylylenes, the presence of the heteroatom in the polymer backbone of polylutidine polymers resulted in surfaces that supported an increased adhesion of primary human umbilical vein endothelial cells (HUVECs). Vapor-based polylutidine coatings are a new class of polymers that feature increased hydrophilicity and increased cell adhesion without limiting the flexibility in selecting appropriate functional side groups.

Introduction

Reactive polymer coatings are of major interest for many applications, ranging from biotechnology to heterogeneous catalysis.^[1] Chemical vapor deposition (CVD) polymerization based on the Gorham process is a convenient and substrate-independent process to synthesize stable, reactive coatings.^[2–6] FDA-approved in some instances,^[7] poly-*p*-xylylene-based coatings have been prepared by CVD polymerization of [2.2]paracyclophane derivatives for surface modification and structuring of a wide range of materials.^[8,5,9] The presence of substituents such as aldehyde, ketone, alcohol, ester, amine, as well as fluorinated groups, thiol reactive groups, ATRP initiator groups, photosensitive or alkynyl groups in the precursor and consequently in the polymer coating has enabled various post-modification strategies.^[2,10–23] Attachment of proteins, short peptides, nucleotides, and other small biologically active molecules onto this functional coating can dramatically influence the response of adherent cells.^[10,11,13,19] Therefore, precise design of surface chemistry provided by CVD enables the control of cell behavior by tailoring interactions between CVD coatings and living organisms.^[24] However, strategies taking advantage of the Gorham process to deposit vapor-based reactive coatings have so far almost always been limited to poly-*p*-xylylenes, that is,

entirely carbon-based polymer backbones with prominent hydrophobicity.^[3] In principle, the high degree of hydrophobicity can be mitigated by replacing one or two of the benzene rings with a heteroaromatics. In particular, electron-withdrawing heteroatoms, such as nitrogen, can introduce additional polarity into the polymer backbone, while still being able to conserve the chemical flexibility of the poly-*p*-xylylene platform. Compared to the extensive literature related to functional [2.2]paracyclophane precursors for CVD polymerization, very little is known about synthetic pathways to functional heterophane precursors.^[25–27] An example of a dimeric heterophane that features a nitrogen heterocycle instead of benzene is [2](1,4)benzo[2](2,5)pyridinophane (pyridinophane **1**), which was first mentioned in literature in 1972, although the compound was obtained only in poor yields of 1%.^[28] In 1973, an improved synthesis with better yields (60%) was reported.^[29] An alternative synthesis from commercially available precursors was reported by Vögtle et al.^[27] but it was only recently, that a simplification of this synthetic route with multigram yields was published.^[26] In 1995, Itoh and co-workers carried out the first CVD polymerization of unfunctionalized heterophanes; this process yielded tough polymer films, probably due to considerable crosslinking.^[30] Herein, we report a new synthetic approach towards chemically active polylutidine surfaces. Impor-

[a] Dr. F. Bally-Le Gall,⁺ C. Hussal,⁺ Prof. Dr. J. Lahann
Institute of Functional Interfaces
Karlsruhe Institute of Technology, Hermann-von-Helmholtz-Platz 1
76344 Eggenstein-Leopoldshafen (Germany)

[b] Dr. F. Bally-Le Gall^{*}
Institute of Materials Science of Mulhouse, UMR 7361
UHA CNRS, University of Strasbourg, 68057 Mulhouse Cedex (France)

[c] Dr. J. Kramer, Prof. Dr. S. Bräse
Institute of Organic Chemistry, Karlsruhe Institute of Technology
Fritz-Haber-Weg 6, 76131 Karlsruhe (Germany)
E-mail: stefan.bräse@kit.edu

[d] K. Cheng, R. Kumar, Dr. T. Eyster, Dr. A. Baek, Prof. Dr. J. Lahann
Biointerfaces Institute and Departments of Biomedical Engineering
and Chemical Engineering
University of Michigan, 2800 Plymouth Road
Ann Arbor, MI 48109 (USA)
E-mail: lahann@umich.edu

[e] V. Trouillet
Institute for Applied Materials, and Karlsruhe Nano Micro Facility
Karlsruhe Institute of Technology, Hermann-von-Helmholtz-Platz 1
76344 Eggenstein-Leopoldshafen (Germany)

[f] Dr. M. Nieger
Department of Chemistry, University of Helsinki
P.O. Box 55, 00014 Helsinki (Finland)

[g] Prof. Dr. S. Bräse
Institute of Toxicology and Genetics
Karlsruhe Institute of Technology, Hermann-von-Helmholtz-Platz 1
76344 Eggenstein-Leopoldshafen (Germany)

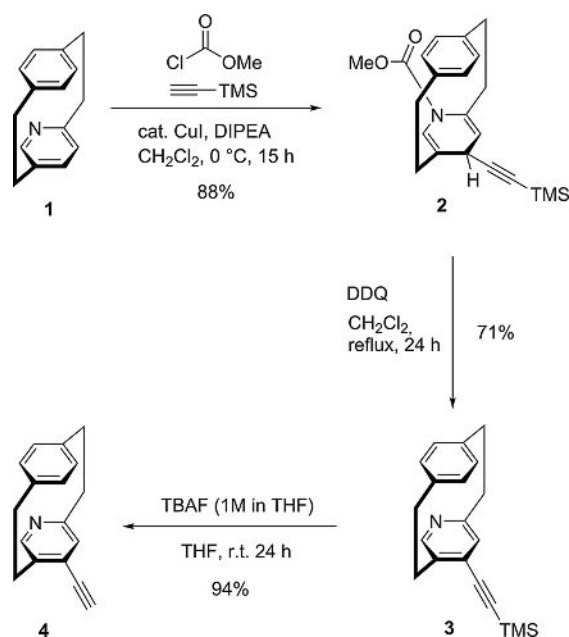
[*] These authors contributed equally to this work.

Supporting information for this article can be found under:
<https://doi.org/10.1002/chem.201700901>.

tantly, the development of a scalable synthesis route of substituted pyridinophanes allowed us to investigate the CVD polymerization of pyridinophane **1** and ethynylpyridinophane **4**. We were able to regioselectively prepare the alkynylated pyridine precursor in an efficient way that can provide sufficient quantities for the CVD polymerization.

Results and Discussion

The synthesis of pyridinophane **1** was carried out according to a recently reported synthesis starting from commercially available 2,5-pyridinedicarboxylic acid.^[26] In brief, after an esterification of the dicarboxylic acid, subsequent treatment with NaBH₄, and bromination afforded one building block for the pyridinophane scaffold. Finally, the cyclophane formation with a dithiol and a photolytic dethionation resulted in pyridinophane **1**. In our hands, the five-step synthesis resulted in improved yields of 37% as compared to the literature-reported yield of 19%.^[26] To date, the only known functionalization method of the heterophane scaffold is the introduction of a nitrile group in *ortho*-position to the nitrogen through a cyanation reaction of the pyridinophane *N*-oxide with trimethylsilyl cyanide.^[25–27] Thus, for the synthesis of pyridinophanes with substituents other than nitrile, such as the alkyne-substituted pyridinophane **4**, a new synthesis route had to be developed. A common method for the alkylation of pyridines is the metal-catalyzed cross-coupling reaction, which requires halogenated or metalated pyridine derivatives. Because neither halogenation nor metalation is known in literature for pyridinophane **1**, we decided to pursue a reductive functionalization through addition of nucleophiles to in situ generated *N*-alkoxycarbonyl pyridinium salts. We took advantage of the fact that copper(I)-catalyzed coupling of acetylenes with pyridines in the presence of an acid chloride or chloroformate activator can result in *ortho*-alkynyl products, even at room temperature.^[31,32] Once synthesized, the resulting alkynylated dihydropyridine derivatives can be re-aromatized to the corresponding pyridines by oxidation with chloranil^[33] or 2,3-dichloro-5,6-dicyano-1,4-benzoquinone (DDQ).^[34] While the alkylation proceeds regioselectively in 2-position for unsubstituted pyridine, a mixture of 1,2-, 1,4-, and 1,6-alkynylated adducts is reported for 3-substituted pyridines.^[34,33] The ratio of regioisomers is significantly influenced by the substituent. Electron-withdrawing substituents predominantly yield 1,2-adducts. The alkylation of higher-substituted pyridines with this method has only been reported for 3,5-dimethylpyridine in low yields.^[34] Due to the presence of a nitrogen atom, compound **1** is an electron-poor aromatic, and, compared to 2,5-disubstituted pyridine, it is a sterically more demanding and rigid molecule. We thus activated compound **1** prior to the addition of the nucleophile to further enhance the regioselectivity for the *para*-alkynylated product (Scheme 1A). In addition, the introduction of the alkoxycarbonyl group at the nitrogen atom sterically inhibited the alkylation at the *ortho*-position. For the subsequent alkylation, the reaction temperature played a crucial role and increasing the temperature from –78 °C to 0 °C resulted in significantly higher yields. In our synthesis, the easy to handle tri-



Scheme 1. Three-step synthesis of ethynylpyridinophane **4** starting from pyridinophane **1**.

methylsilyl-protected acetylene was used as the alkyne source. After optimization of the reaction conditions, we were able to conduct the copper(I)-catalyzed alkylation with trimethylsilylacetylene at room temperature yielding the *para*-alkynylated dihydropyridinophane **2** in excellent yields (88%) as a single diastereomer. Under these conditions (see the Supporting Information), only traces of the *ortho*-alkynylated adduct were observed. Subsequent re-aromatization of **2** DDQ yielded the trimethylsilylethynyl pyridinophane **3**. Final cleavage of the trimethylsilyl moiety with TBAF gave the desired alkynylated pyridinophane **4** in excellent yield over three steps. The regioselectivity of the synthesis for the *para*-substituted pyridinophane was unambiguously proven by the X-ray structure of the final ethynylpyridinophane **4** (Figure 1). Next, we investigated the CVD polymerization of unfunctionalized pyridinophane **1**, ethy-

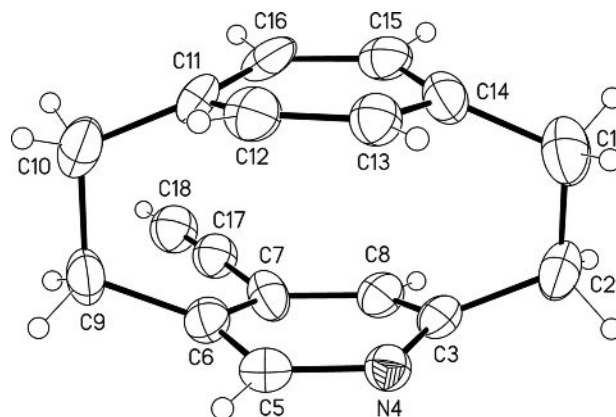
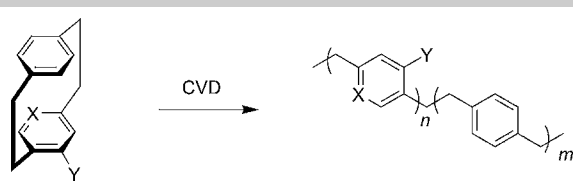


Figure 1. The molecular structure of ethynylpyridinophane **4**, determined by crystal structure analysis. Displacement parameters are drawn at 50% probability level, minor disordered part omitted for clarity.

Table 1. Synthesis of poly(*p*-xylylene) **7** and **8** and poly(2,5-lutidinylene-*co-p*-xylylene) **9** and **10** coatings by CVD polymerization.



Polymer	X	Y
7	CH	H
8	CH	CCH
9	N	H
10	N	CCH

nylpyridinophane **4** (Table 1; polymers **7–10**) and their corresponding, literature-known, [2.2]paracyclophane analogues (**5** and **6**). Briefly, the CVD process consisted of sublimation of the phane derivative at approximately 100 °C, followed by its pyrolysis at a temperature between 510 and 660 °C, depending on the precursor. Spontaneous polymerization of the reactive intermediates occurred during deposition onto a rotating and cooled (15 °C) sample holder. The whole process occurred under reduced pressure in a custom-built CVD set-up. Film thicknesses ranged between 25–65 nm, as measured by ellipsometry. Control of polymerization conditions, especially pyrolysis temperature, allowed selective cleavage of the ethylene bridges and preserved the integrity of the functional groups. Specially, infrared reflection absorption spectroscopy (IRRAS) confirmed the presence of alkyne groups in polymer **10** after CVD polymerization: As shown in Figure 2, the IR spectrum re-

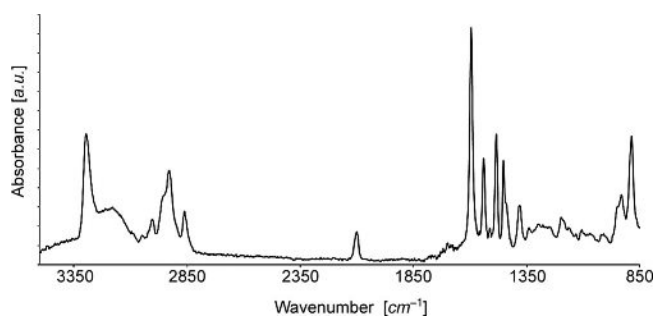
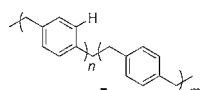
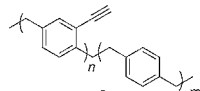
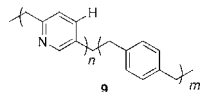
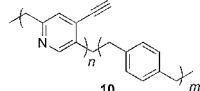


Figure 2. IRRAS spectrum of polymer **10** coating prepared by CVD polymerization of ethynylpyridinophane **4**.

veals two characteristic bands corresponding to $\equiv\text{C-H}$ bond elongation (3292 cm^{-1}) and $\text{C}\equiv\text{C}$ bond deformation (2099 cm^{-1}). In addition, the bands at $2823\text{--}3031\text{ cm}^{-1}$ indicate the presence of the lutidinylene and xylylene units. Symmetric and asymmetric C–H stretching modes are characteristic in this region ($2823\text{--}3031\text{ cm}^{-1}$).

Chemical composition of the synthesized polymer coatings was further confirmed by X-ray photoelectron spectroscopy (XPS) (Table 2). XPS measurements revealed the presence of nitrogen atom in polymer **9** (6.9 at.%) and polymer **10** (6.2 at.%). The values are in good agreement with theoretical amounts

Table 2. Chemical composition of polymers **7**, **8**, **9**, **10** in at.% as determined by XPS measurements of the polymer films deposited on gold substrates (calculated theoretical compositions are included for comparison.)

	C–C/H	C–N/[O]	C–N	Residual O
B.E. [eV]	285.0	285.8 ± 0.2	399.2 ± 0.2	532.8 ± 0.2
	98.6 (100)	–	–	1.4 (0)
	99.6 (100)	–	–	0.4 (0)
	83.2 (81.3)	9.3 (12.5)	6.9 (6.3)	0.7 (0)
	72.7 (83.3)	19.1 (11.1)	6.2 (5.6)	2.0 (0)

(6.3 at.% and 5.6 at.%, respectively), calculated by on the basis of statistical copolymers with 2,5-lutidinylene and *p*-xylylene repeating units (see also Figure 2 in the Supporting Information). These polymer coatings had low oxygen content (0.7 at.% and 2.1 at.%, respectively), implying the saturation of free polymer radicals on surface after the CVD polymerization. Peak fitting of the high resolution peak C 1s signals revealed that the polymers were comprised of carbon atoms with different chemical states. The C 1s spectra were in accordance with a peak that corresponds to the binding energy of C–C/H bonds, set to be 285.0 eV, and one peak at 285.8 eV, which can be attributed to the binding energy of C–N bonds. Not surprisingly, poly(2,5-lutidinylene-*co-p*-xylylene) coatings have a higher wettability than poly(*p*-xylylene) coatings, because lutidinylene units display a higher polarity than xylylenes. Contact angle measurements indicated that the 2,5-lutidinylene-*co-p*-xylylene-based coatings were more hydrophilic than *p*-xylylene-based coatings (average of 69° in comparison with 89° respectively). Furthermore, the nitrogen atom has a lone pair of electrons; as a result, it can act as a Lewis base and create a partial charge on the surface. Such properties are usually of interest when cell adhesion to a surface is desired. We have previously observed that non-functionalized poly-*p*-xylylene coatings generally display limited promotion of cell adhesion, whereas coatings with more polar side groups support cell adhesion.^[35] However, it is very difficult to predict general trends for cell adhesion to a surface based on simplified considerations of hydrophobicity^[36–38] or the nature of the charge present on the surface.^[39] It is also critical to attempt to decouple surface charge from surface wettability to independently study their effects on cell adhesion. Therefore, we hypothesized that the conversion of the aromatic carbon to a nitrogen in the polymer backbone endows poly(2,5-lutidinylene-*co-p*-xylylene) coatings with a partially positive charge, which could enhance cell adhesion and spreading over those cultured on par-

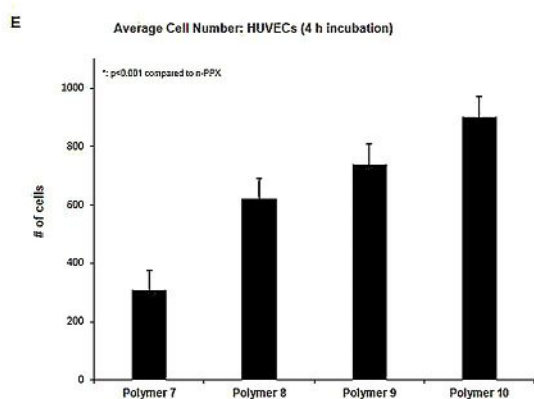
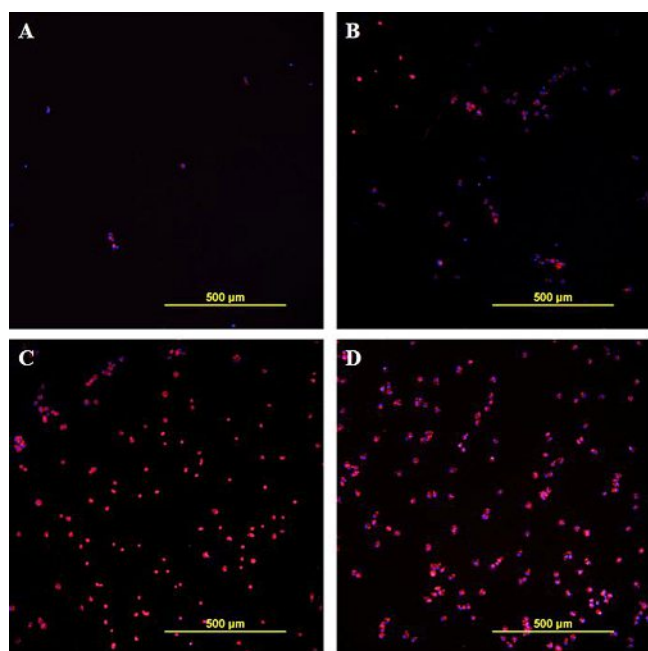


Figure 3. Fluorescence microscopy of HUVECs cultured for four hours and stained with phalloidin/DAPI on A) polymer 7, B) polymer 8, C) polymer 9 and D) polymer 10 and E) quantification of the number of cells for three images taken per substrate and averaged (three trials combined) for both nonfunctionalized (polymers 7 and 9) and alkyne-functionalized substrates (polymers 8 and 10).

ylene coatings. To probe this hypothesis, primary human umbilical vein endothelial cells (HUVECs) were thus cultured on the different polymer coatings in serum-free media. Figure 3 shows higher cell adhesion for polymers 9 and 10 coatings. HUVECs spread out 2.4 times more on polymer 9 compared to polymer 7. Following a similar trend, the increase in cell adhesion was 1.4 times higher for polymer 10 than to polymer 8. These results confirmed the tendency observed by fluorescence microscopy, since pyridinophane-based coatings show a far higher number of HUVECs attached over paracyclophane-based coatings. We have thus demonstrated how altering even one CH fragment into nitrogen in one of the monomer units of the polymer backbone can drastically change how cells

behave on surface. Streaming potential measurements were performed to compare the ζ -potential of the two non-functionalized polymer coatings (polymer 7 and 9). The results support the hypothesis that the presence of a heteroatom in the polymer backbone improves cell adhesion (Figure 4). The iso-

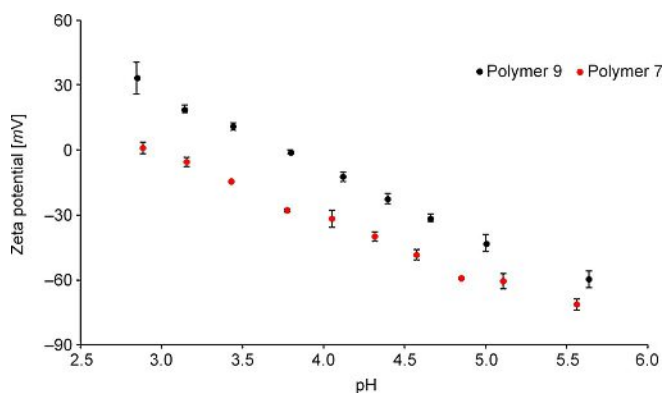


Figure 4. Streaming potential of polymer films 7 (red) and 9 (black). Polymer 9 has an IEP of 3.60, which is higher than that for polymer 7 (2.80). This difference is attributable to the partial positive charge created by the nitrogen atom in the polymer backbone.

electric point (IEP), that is, the pH at which the ζ -potential values reaches zero, is 3.60 and 2.80 for polymers 9 and 7, respectively. This indicates a more positive charge character for the polymer 9 due to the presence of a nitrogen atom in the backbone. Finally, post-modification of pyridinophane-based coatings was conducted to verify the reactivity of poly(4-ethynyl-2,5-lutidinylene-*co-p*-xylylene). Specifically, we employed the copper-catalyzed Huisgen 1,3-dipolar cycloaddition between

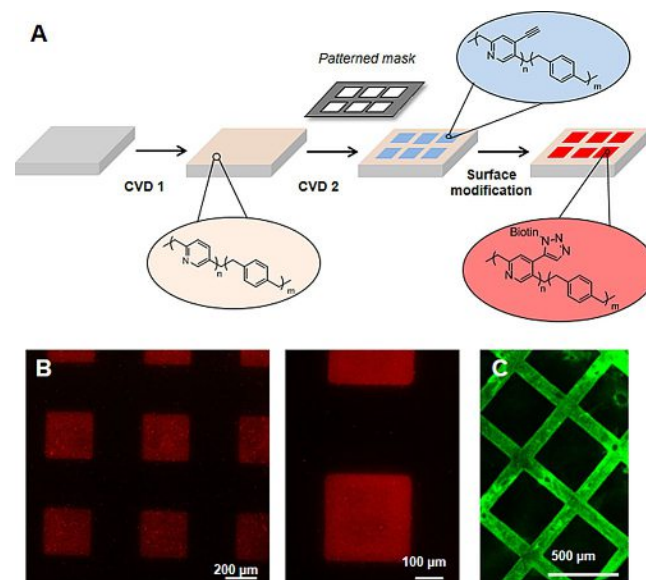


Figure 5. A) Schematic representation of the protocol used for biotin immobilization on the functional coating. B) Fluorescence images after streptavidin incubation and C) fluorescence image after azido-PEG microcontact printing on polymer 10 coating (PEG is located on square pattern in this case) and BSA-FITC incubation.

10 and different azide-containing biomolecules. In a first experiment, the spatially controlled immobilization of PEG-azide on polymer **10** coating was investigated by means of contact printing. Subsequent incubation of fluorescein-labeled bovine serum albumin (BSA-FITC) on the substrate revealed the presence of PEG molecules on parts of the surface. The selective adhesion of BSA to areas not covered with PEG underlines the selectivity of the click reaction (Figure 5C). In a second experiment, a micro-structured coating comprised of a background of polymer **9** and squares of polymer **10** was prepared by vapor-assisted micro-patterning in replica (VAMPIR) process, a two-step CVD process described elsewhere.^[40] In the presence of copper(II) sulfate and sodium ascorbate, the micro-structured substrate reacted with azido-functionalized biotin. The selectivity towards polymer **10** was then revealed through incubation with a fluorescence-labeled streptavidin in a subsequent step (Figure 5A,B). Fluorescence images revealed the presence of streptavidin selectively on the squared patterns, which implies the presence of biotin linked to polymer **10**. The reactivity of the substrate to click chemistry reaction through Huisgen 1,3 dipolar cycloaddition creates numerous pathways for further functionalization of the coating with bioactive moieties, such as peptides and growth factors.

Conclusion

In this work, we report the successful preparation of two novel nitrogen-containing and functionalized polymer coatings by CVD polymerization. A synthetic route to a *para*-alkynylated pyridinophane was initially established that resulted in the synthesis of the precursors with excellent yields. In addition, we have confirmed the stability and integrity of reactive alkyne groups during CVD polymerization, opening new perspectives for the design of new cell culture substrates. These new heterophane-based coatings are uniquely characterized by the presence of nitrogen atoms in the polymer backbone as well as alkyne side groups. The combination of these structural elements resulted in an increased cell spreading and adhesion along with facile access to conjugation of biomolecules.

Experimental Section

General remarks: General information about the analytical equipment, the complete characterizations of all of the compounds including the ¹H and ¹³C NMR spectra, ellipsometry results, IRRAS results, contact angle measurements, XPS spectra, and the crystallographic data can be found in the Supporting Information.

Synthesis and characterization

(rac)-N-Methoxycarbonyl-4-((trimethylsilyl)ethynyl)[2](1,4)benzeno[2](2,5)-4(2H)-pyridinophane (2): Trimethylsilylacetylene (338 μL, 235 mg, 2.39 mmol, 5.00 equiv) and *N,N*-diisopropylethylamine (DIPEA, 413 μL, 309 mg, 2.39 mmol, 5.00 equiv) were added to a suspension of CuI (91.0 mg, 0.478 mmol, 1.00 equiv) in dry CH₂Cl₂ (2 mL) cooled to 0 °C. After stirring for 30 min at 0 °C, the suspension was transferred by syringe to a cold (0 °C) solution of **(rac)-1** (100 mg, 0.478 mmol, 1.00 equiv) in methyl chloroformate

(185 μL, 226 mg, 2.39 mmol, 5.00 equiv). The mixture was stirred at 0 °C for 15 h. The solvent and the volatile reagents were evaporated under reduced pressure and the crude product was purified by column chromatography (cHex/EtOAc 10:1) to yield the substituted dihydropyridinophane **2** (153 mg, 0.419 mmol, 88%) as a colorless oil. *R*_f = 0.36 (cHex/EtOAc 10:1); ¹H-NMR (500 MHz, CDCl₃): δ = 0.06 (s, 9H, Si(CH₃)₃), 2.20–1.15 (m, 1H, H_{pyr}), 2.35–1.31 (m, 1H, H_{pyr}), 2.44–2.48 (m, 1H, H_{pyr}), 2.54–2.60 (m, 1H, H_{pyr}), 2.70–2.76 (m, 1H, H_{pyr}), 2.95 (dd, ³J = 7.5 Hz, ⁴J = 1.1 Hz, 1H, Py-H4), 3.04–3.07 (m, 1H, H_{pyr}), 3.08–3.12 (m, 1H, H_{pyr}), 3.47 (s, 1H, H_{pyr}), 3.78 (s, 3H, OCH₃), 4.53 (d, ³J = 7.5 Hz, 1H, Py-H3), 5.58 (s, 1H, Py-H6), 6.81 (dd, ³J = 7.9 Hz, ⁴J = 1.7 Hz, 1H, Ar-H), 6.86 (dd, ³J = 7.9 Hz, ⁴J = 1.6 Hz, 1H, Ar-H), 6.93 (dd, ³J = 7.9 Hz, ⁴J = 1.3 Hz, 1H, Ar-H), 7.01 ppm (dd, ³J = 7.9 Hz, ⁴J = 1.3 Hz, 1H, Ar-H); ¹³C-NMR (125 MHz, CDCl₃): δ = 0.18 (+, SiCH₃), 27.01 (–, CH₂), 32.00 (–, CH₂), 29.45 (+, C–Py), 33.22 (–, CH₂), 33.52 (–, CH₂), 53.10 (+, OCH₃), 82.79 (C_q, C≡CTMS), 105.40 (C_q, C≡CTMS), 116.26 (C_q, C–Ar/Py), 120.36 (+, C–Ar/Py), 129.46 (+, C–Ar/Py), 129.83 (+, C–Ar/Py), 130.51 (+, C–Ar/Py), 130.98 (+, C–Ar/Py), 131.25 (+, C–Ar/Py), 134.55 (C_q, C–Ar/Py), 138.04 (C_q, C–Ar/Py), 138.83 (C_q, C–Ar/Py), 152.26 ppm (C_q, CO); FT-IR (ATR): $\tilde{\nu}$ = 2926 (w), 2852 (w), 2164 (w) [C≡C], 1712 (m) [C=O], 1681 (w), 1639 (w), 1503 (w), 1439 (m), 1380 (w), 1344 (m), 1311 (m), 1289 (w), 1270 (w), 1247 (m), 1175 (w), 1137 (w), 1087 (w), 1060 (w), 1013 (w), 997 (w), 952 (w), 890 (w), 836 (m), 802 (w), 758 (m), 718 (w), 696 (w), 628 (w), 581 (w), 535 (w), 515 (w), 450 (w), 405 cm^{–1} (w); MS (70 eV, FAB): *m/z* (%): 365 (100) [M⁺], 262 (11), 261 (38), 138 (15), 137 (25), 136 (34), 107 (10), 89 (12); HRMS calcd for C₂₂H₂₇NO₂Si: 365.181; found 365.1814.

(rac)-4-((Trimethylsilyl)ethynyl)[2](1,4)benzeno[2](2,5)pyridinophane (3): 2,3-Dichloro-5,6-dicyano-1,4-benzoquinone (DDQ, 306 mg, 1.35 mmol, 3.00 equiv) was added to a solution of **2** (164 mg, 0.449 mmol, 1.00 equiv) in dry CH₂Cl₂ (8 mL) and the reaction mixture was stirred at reflux for 24 h. The reaction mixture was quenched with a 2 M aqueous solution of NaOH, the aqueous phase was extracted with CH₂Cl₂ (4 × 20 mL) and the combined organic phases were washed with brine (2 × 20 mL). After drying over MgSO₄, the solvent was removed under reduced pressure and the crude product was purified by column chromatography (cHex/EtOAc 2:1) to yield the 4-TMS-ethynylpyridinophane **3** (96.9 mg, 0.318 mmol, 71%) as a colorless solid. *R*_f = 0.21 (cHex/EtOAc 2:1); m.p. 204 °C; ¹H-NMR (400 MHz, CDCl₃): δ = 0.33 (s, 9H, Si(CH₃)₃), 2.74–2.82 (m, 1H, H_{pyr}), 3.04–3.21 (m, 5H, H_{pyr}), 3.26–3.33 (m, 1H, H_{pyr}), 3.42–3.48 (m, 1H, H_{pyr}), 6.40 (s, 1H, Py-H3), 6.44 (dd, ³J = 7.8 Hz, ⁴J = 1.9 Hz, 1H, Ar-H), 6.59 (dd, ³J = 7.9 Hz, ⁴J = 1.9 Hz, 1H, Ar-H), 6.82–6.84 (m, 2H, Ar-H), 7.70 ppm (s, 1H, Py-H6); ¹³C-NMR (100 MHz, CDCl₃): δ = 0.00 (+, SiCH₃), 31.76 (–, CH₂), 34.00 (–, CH₂), 34.63 (–, CH₂), 36.82 (–, CH₂), 102.52 (C_q, 2 × C≡CTMS), 126.90 (+, C–Ar/Py), 129.63 (+, C–Ar/Py), 131.81 (+, C–Ar/Py), 132.04 (C_q, C–Ar/Py), 133.11 (+, C–Ar/Py), 133.43 (+, C–Ar/Py), 134.71 (C_q, C–Ar/Py), 138.82 (C_q, C–Ar/Py), 139.89 (C_q, C–Ar/Py), 153.26 (+, C–Py), 160.22 ppm (C_q, C–Py); FT-IR (ATR): $\tilde{\nu}$ = 2956 (w), 2926 (w), 2850 (w), 2153 (w) [C≡C], 1569 (m), 1520 (w), 1501 (w), 1465 (w), 1432 (w), 1412 (w), 1376 (w), 1323 (w), 1247 (m), 1158 (w), 1142 (w), 1119 (w), 1094 (w), 971 (w), 934 (w), 877 (m), 837 (m), 797 (m), 757 (m), 744 (m), 721 (m), 697 (m), 649 (m), 594 (m), 552 (w), 538 (m), 499 (m), 410 cm^{–1} (w); MS (70 eV, EI): *m/z* (%): 305 (54) [M⁺], 201 (15), 186 (28), 133 (23), 104 (50), 103 (13), 89 (60), 88 (12), 87 (21), 78 (11), 77 (19), 73 (16), 59 (15), 45 (100), 44 (12), 43 (17); HRMS calcd for C₂₀H₂₃NSi: 305.1600; found 305.1598.

(rac)-4-(Ethynyl)[2](1,4)benzeno[2](2,5)pyridinophane (4): Tetra-butylammonium fluoride (TBAF, 1 M solution in THF, 310 μL, 280 mg, 0.310 mmol, 1.00 equiv) was slowly added to a solution of **3** (94.6 mg, 0.310 mmol, 1.00 equiv) in dry THF (2 mL) and the reac-

tion mixture was stirred at room temperature for 24 h. The solvent was removed under reduced pressure and the crude product was dissolved in ethyl acetate. The organic phase was washed with water, dried over MgSO_4 and the solvent removed under reduced pressure. The crude product was purified by column chromatography (cHex/EtOAc 2:1) to yield 4-ethynylpyridinophane (**4**) (68.1 mg, 0.292 mmol, 94%) as a colorless solid. $R_f = 0.23$ (cHex/EtOAc 2:1); m.p. 204 °C; $^1\text{H-NMR}$ (400 MHz, CDCl_3): $\delta = 2.78\text{--}2.86$ (m, 1H, H_{pyr}), 3.07–3.19 (m, 5H, H_{pyr}), 3.28–3.34 (m, 1H, H_{pyr}), 3.43–3.50 (m, 1H, H_{pyr}), 3.44 (s, 1H, CCH), 6.43 (dd, $^3J = 7.8$ Hz, $^4J = 1.8$ Hz, 1H, Ar–H), 6.46 (s, 1H, Py–H3), 6.61 (dd, $^3J = 7.8$ Hz, $^4J = 1.8$ Hz, 1H, Ar–H), 6.82–6.86 (m, 2H, Ar–H), 7.72 ppm (s, 1H, Py–H6); $^{13}\text{C-NMR}$ (100 MHz, CDCl_3): $\delta = 31.54$ (–, CH_2), 34.13 (–, CH_2), 34.63 (–, CH_2), 36.83 (–, CH_2), 81.22 (C_{q} , $\text{C}\equiv\text{CH}$), 84.16 (+, $\text{C}\equiv\text{CH}$), 127.38 (+, C–Ar/Py), 129.88 (+, C–Ar/Py), 131.10 (C_{q} , C–Ar/Py), 131.83 (+, C–Ar/Py), 133.20 (+, C–Ar/Py), 133.47 (+, C–Ar/Py), 134.83 (C_{q} , C–Ar/Py), 138.83 (C_{q} , C–Ar/Py), 139.91 (C_{q} , C–Ar/Py), 153.43 (+, C–Py), 160.36 ppm (C_{q} , C–Py); FT-IR (ATR): $\tilde{\nu} = 3076$ (w), 2959 (w), 2926 (w), 2852 (w), 2089 (w), 1902 (w), 1576 (w), 1526 (w), 1501 (w), 1469 (w), 1448 (w), 1433 (w), 1412 (w), 1376 (w), 1319 (w), 1294 (w), 1260 (w), 1204 (w), 1185 (w), 1138 (w), 1114 (w), 967 (w), 920 (w), 888 (w), 865 (w), 796 (w), 763 (w), 743 (w), 719 (w), 679 (w), 595 (w), 551 (w), 537 (w), 495 (w), 483 (w), 447 cm^{-1} (w); MS (70 eV, EI): m/z (%): 233 (100) [M^+], 232 (10), 104 (95), 103 (10), 58 (12), 43 (34); HRMS calcd for $\text{C}_{17}\text{H}_{15}\text{N}$: 233.1204; found 233.1206.

Fabrication of reactive coatings by chemical vapor deposition polymerization (CVD)

[2.2]Paracyclophane **5** was used as received. 4-Ethynyl[2.2]paracyclophane **6**^[41] and pyridinophane **1**^[26] were synthesized according to protocols described in literature. Ethynylpyridinophane **4** was synthesized as described above. Poly(*p*-xylylene) (polymer **7**), poly(4-ethynyl-*p*-xylylene-co-*p*-xylylene) (polymer **8**), poly(2,5-lutidinylene-co-*p*-xylylene) (polymer **9**), poly(4-ethynyl-2,5-lutidinylene-co-*p*-xylylene) (polymer **10**) were synthesized by chemical vapor deposition polymerization of the respective above-mentioned precursors. Precursors were sublimated at a temperature above 100 °C under low pressure (<0.2 mbar) before being transferred in a pyrolysis furnace, maintained at a temperature T_{pyr} (polymer **7**, **8** and **9** at 660 °C, polymer **10** at 510 °C) in a stream of argon gas (20 sccm). Polymerization of the precursors spontaneously occurred by vapor deposition on the substrate, kept at 15 °C and rotating to get a uniform thickness of the polymer film in the deposition chamber.

Micro-structured pyridinophane coatings were prepared by the previously reported VAMPIR technique^[11] in order to fabricate micro-structured coatings containing square patterns of polymer **9** and **10**. For this purpose, a ground layer of polymer **9** was first homogeneously coated on the substrate, according to the above mentioned CVD polymerization conditions. Then, a patterned PDMS microstencil (squares of 300 $\mu\text{m} \times 300 \mu\text{m}$), fabricated as previously described^[11] was placed on the ground polymer and a second layer of polymer **10** was subsequently deposited onto the surface not covered by the microstencil to generate the micropatterns.

Surface characterization of CVD coatings: ellipsometry, IRRAS, contact angle and XPS

Thickness of the polymer coatings was measured using a multi-wavelength rotating analyzer ellipsometer M-44 (J.A. Woollam, USA) at an incident angle of 75°. Data were analyzed using

WVASE32 software and modelled as a Cauchy material. Thickness values correspond to the average thickness of triplicates. Infrared reflection absorption spectroscopy (IRRAS) spectra were recorded on a VERTEX 80 V spectrometer (Bruker, Germany) at a grazing angle of 80°. Sessile drop (Millipore) water contact angles were measured with a custom-built contact angle goniometer equipped with a CCD video capture apparatus (EHD imaging, Germany) under ambient conditions with the tip not being in contact with the droplet. Measurements were made on both sides of the drop and were averaged. Each result is the average value of more than twenty measurements (performed on various samples coming from different CVD runs). XPS measurements were performed using a K-Alpha XPS spectrometer (ThermoFisher Scientific, East Grinstead, UK). Data acquisition and processing using the Thermo Advantage software is described elsewhere.^[42] All polymer thin films were analyzed using a microfocused, monochromated Al K_{α} X-ray source (400 μm spot size). The kinetic energy of the electrons was measured by a 180° hemispherical energy analyzer operated in the constant analyzer energy mode (CAE) at 50 eV pass energy for elemental spectra. The spectra were fitted with one or more Voigt profiles (B.E. uncertainty: ± 0.2 eV) and Scofield sensitivity factors were applied for quantification.^[43] All spectra were referenced to the C 1s peak at 285.0 eV binding energy (C–C, C–H) controlled by means of the known photoelectron peaks of metallic Cu, Ag, and Au, respectively.

Streaming potential measurements

In order to ascertain whether polymer **9** had a higher isoelectric point than polymer **7**, ζ -potential measurements were collected at various values of pH. Measurements were conducted using the SurPASS electrokinetic analyzer (Anton Paar GmbH, Graz, Austria) in the asymmetric mode with a polypropylene surface being used as the reference. Streaming current readings were captured at a pressure of 200 mbar and a flow rate of 60–70 mL min^{-1} was observed. A pH range of 3 to 6 was explored in increments of 0.3. Titration was performed using an automated unit from a starting value of 6 to a final value of 3 using 0.1 M hydrochloric acid as the titrant and 0.001 M potassium chloride solution as the electrolyte. The electrolyte solution was stirred continuously and also purged continuously with nitrogen to prevent carbon dioxide dissolution, which would cause undesirable changes in the pH value. Samples were rinsed for 3 minutes before each measurement to equilibrate the surface against the electrolyte solution. After the streaming current was measured using Ag/AgCl electrodes, Helmholtz-Smoluchowski equation was used to obtain the ζ -potentials.

Surface immobilization and visualization by fluorescence microscopy

For biotin immobilization, micro-structured substrates were immersed in an aqueous solution of copper sulphate (1 mM), sodium ascorbate (3 mM) and Biotin-dPEG7-azide (16 μM) for 18 h at room temperature. Substrates were rinsed with DI-water and with buffer solution (0.02% (v/v) Tween 20 and 0.1% (w/v) bovine serum albumin (BSA) in phosphate buffered saline (PBS, pH 7.4)). Then, streptavidin incubation was performed by immersing the substrates in rhodamine-labeled streptavidin solution (10 $\mu\text{g} \times \text{mL}^{-1}$ in buffer solution) for 1 h at room temperature. Substrates were rinsed with buffer solution and distilled water and were soaked in distilled water for 1 h. Fluorescence micrographs were recorded using a Nikon Eclipse 90i fluorescence microscope. For poly(ethylene glycol) (PEG) immobilization, patterned PDMS stamps (squares of 350 \times 350 μm) were fabricated as previously described^[44] and were

oxidized for 20 min using a UV-ozone cleaner (Jelight Co. Inc) before use. The stamps were inked with an aqueous solution of copper sulfate (0.1 mM), sodium ascorbate (100 mM) and azido-mPEG5k (10 mg mL⁻¹). Then, they were kept in contact with homogeneously polymer-10-coated samples overnight and substrates were rinsed thoroughly with distilled water. Afterwards, substrates were immersed in a solution of fluorescein-conjugated BSA (BSA-FITC, 0.5 mg mL⁻¹ in PBS) for 3 h. Substrates were rinsed with PBS and distilled water. Fluorescence micrographs were recorded using a Nikon E800 fluorescence microscope.

Cell culture experiments: endothelial cell adhesion, image and statistical analysis

Primary human umbilical vein endothelial cells (HUVECs) were obtained as a kind gift from the Pinsky lab. Homogeneously coated silicon substrates were placed into a 24-well plate. After trypsonization, 30,000 cells in Medium 199 (no serum) were added to each well, and the cells were allowed to incubate for 4 h. After incubation, the surfaces were fixed with 4% formaldehyde in PBS, then stained with phalloidin and mounted with DAPI-containing Pro-Long Gold for imaging with an Olympus BX-51 fluorescence microscope. Samples were run in triplicate. The software package ImageJ (NIH) was used to analyze images. Normalized cell spreading was quantified by measuring the total cell area and dividing by the total number of cells (counted by DAPI spot). Magnitude of fluorescence quantification was performed by converting the images to a 32-bit gray scale and then measuring the mean gray value. All error bars represent standard error (one standard deviation from the mean divided by the square root of the total number of images averaged). Statistical significance was determined using Students two-tailed T-test assuming unequal variance, with $p < 0.05$ considered significant.

Crystal structure determination of ethynylpyridinophane 4

The single-crystal X-ray diffraction study was carried out on a Nonius KappaCCD diffractometer at 123(2) K using Mo-K α radiation ($\lambda = 0.71073$ Å; Direct Methods (SHELXS-97)^[45] were used for structure solution and refinement was carried out using SHELXL-98 (full-matrix least-squares on F^2).^[45] Hydrogen atoms were refined using a riding model. The absolute structure could not be determined reliably either by refinement of Flack's x -parameter $x = -7(8)$ ^[46] nor using Bayesian statistics on Bijvoet differences (Hooft's y -parameter $y = 0.6(14)$).^[47] There is a disorder of the ethynylpyridine versus the benzene ring (approx. 2:1: (0.684(4):0.316(4)) about a mirror plane (for details see the cif-file). Colorless crystals, C₁₇H₁₅N, $M_r = 233.30$, crystal size 0.30 × 0.20 × 0.10 mm, monoclinic, space group C2 (No. 5), $a = 15.3179(9)$ Å, $b = 7.5135(5)$ Å, $c = 11.3255(6)$ Å, $\beta = 95.508(5)^\circ$, $V = 1297.45(13)$ Å³, $Z = 4$, $\rho = 1.194$ Mg m⁻³, $\mu(\text{Mo-K}\alpha) = 0.069$ mm⁻¹, $F(000) = 496$, $2\theta_{\text{max}} = 50.0^\circ$, 6440 reflections, of which 2276 were independent ($R_{\text{int}} = 0.062$), 156 parameters, 4 restraints $R1 = 0.063$ (for 1935 $I > 2\sigma(I)$), $wR2 = 0.162$ (all data), $S = 1.03$, largest diff. peak/hole = 0.255/−0.211 e Å⁻³, $x = -7(8)$, $y = 0.6(14)$. CCDC 1519800 (4) contains the supplementary crystallographic data. These data can be obtained free of charge by The Cambridge Crystallographic Data Centre

Acknowledgements

The authors acknowledge funding from the Helmholtz Association within the BioInterfaces Program of the KIT. C.H., S.B.; and J.L. thank the German Science Foundation (DFG) for financial

support within the frame of the collaborative research center SFB 1176 (project B3). J.L. and R.K. acknowledge support from the Defense Threat Reduction Agency (DTRA) through Grant HDTRA1-12-1-0039 as a part of the interfacial dynamics and reactivity program. J.L. and R.K. are also grateful to the Army Research Office (ARO) for funding provided under Grant W911NF-11-1-0251. Annamarija Raic is gratefully acknowledged for designing the frontispiece artwork.

Conflict of interest

The authors declare no conflict of interest.

Keywords: alkynes • chemical vapor deposition • click chemistry • pyridinophanes • reactive coatings

- [1] D. G. Castner, B. D. Ratner, *Surf. Sci.* **2002**, *500*, 28.
- [2] M. E. Alf, A. Asatekin, M. C. Barr, S. H. Baxamusa, H. Chelawat, G. Ozaydin-Ince, C. D. Petruczuk, R. Sreenivasan, W. E. Tenhaeff, N. J. Trujillo, S. Vaddiraju, J. Xu, K. K. Gleason, *Adv. Mater.* **2010**, *22*, 1993.
- [3] J. B. Fortin, T. M. Lu, *Chemical Vapor Deposition Polymerization: The Growth and Properties of Parylene Thin Films*, Springer Science+Business Media, LLC, New York, **2004**.
- [4] W. F. Gorham, *J. Polym. Sci., Part A-1: Polym. Chem.* **1966**, *4*, 3027.
- [5] H. Hopf, *Angew. Chem. Int. Ed.* **2008**, *47*, 9808; *Angew. Chem.* **2008**, *120*, 9954.
- [6] I. E. Paulus, M. Heiny, V. P. Shastri, A. Greiner, *Polym. Chem.* **2016**, *7*, 54.
- [7] A. O. Ragheb, B. L. Bates, N. E. Fearnot, T. G. Kozma, W. D. Voorhees, A. H. Gershlick, U.S. Patent 6774278, **2004**.
- [8] A. K. Bier, M. Bognitzki, J. Mogk, A. Greiner, *Macromolecules* **2012**, *45*, 1151.
- [9] C. Y. Wu, H. Y. Sun, W. C. Liang, H. L. Hsu, H. Y. Ho, Y. M. Chen, H. Y. Chen, *Chem. Commun.* **2016**, *52*, 3022.
- [10] F. Bally, K. Cheng, H. Nandivada, X. Deng, A. M. Ross, A. Panades, J. Lahann, *ACS Appl. Mater. Interfaces* **2013**, *5*, 9262.
- [11] H.-Y. Chen, J. Lahann, *Langmuir* **2011**, *27*, 34.
- [12] H.-Y. Chen, T.-J. Lin, M.-Y. Tsai, C.-T. Su, R.-H. Yuan, C.-C. Hsieh, Y.-J. Yang, C.-C. Hsu, H.-M. Hsiao, Y.-C. Hsu, *Chem. Commun.* **2013**, *49*, 4531.
- [13] Y.-C. Chen, T.-P. Sun, C.-T. Su, J.-T. Wu, C.-Y. Lin, J. Yu, C.-W. Huang, C.-J. Chen, H.-Y. Chen, *ACS Appl. Mater. Interfaces* **2014**, *6*, 21906.
- [14] X. Deng, T. W. Eyster, Y. Elkasabi, J. Lahann, *Macromol. Rapid Commun.* **2012**, *33*, 640.
- [15] X. Deng, C. Friedmann, J. Lahann, *Angew. Chem. Int. Ed.* **2011**, *50*, 6522; *Angew. Chem.* **2011**, *123*, 6652.
- [16] Z.-Y. Guan, C.-Y. Wu, Y.-J. Li, H.-Y. Chen, *ACS Appl. Mater. Interfaces* **2015**, *7*, 14431.
- [17] Y. Liang, J. H. Jordahl, H. Ding, X. Deng, J. Lahann, *Chem. Vap. Deposition* **2015**, *21*, 288.
- [18] H. Nandivada, H. Y. Chen, L. Bondarenko, J. Lahann, *Angew. Chem. Int. Ed.* **2006**, *45*, 3360; *Angew. Chem.* **2006**, *118*, 3438.
- [19] H. Y. Sun, C. Y. Fang, T. J. Lin, Y. C. Chen, C. Y. Lin, H. Y. Ho, M. H. C. Chen, J. S. Yu, D. J. Lee, C. H. Chang, H. Y. Chen, *Adv. Mater. Interfaces* **2014**, *1*, 1400093.
- [20] T. P. Sun, C. H. Tai, J. T. Wu, C. Y. Wu, W. C. Liang, H. Y. Chen, *Biomater. Sci.* **2016**, *4*, 265.
- [21] B. Waterkotte, F. Bally, P. M. Nikolov, A. Waldbaur, B. E. Rapp, R. Truckenmüller, J. Lahann, K. Schmitz, S. Giselbrecht, *Adv. Funct. Mater.* **2014**, *24*, 442.
- [22] J.-T. Wu, C.-H. Huang, W.-C. Liang, Y.-L. Wu, J. Yu, H.-Y. Chen, *Macromol. Rapid Commun.* **2012**, *33*, 922.
- [23] J. T. Wu, T. P. Sun, C. W. Huang, C. T. Su, C. Y. Wu, S. Y. Yeh, D. K. Yang, L. C. Chen, S. T. Ding, H. Y. Chen, *Biomater. Sci.* **2015**, *3*, 1266.
- [24] M. Yoshida, R. Langer, A. Lendlein, J. Lahann, *J. Macromol. Sci. Polym. Rev.* **2006**, *46*, 347.
- [25] A. Fürstner, M. Alcarazo, H. Krause, C. W. Lehmann, *J. Am. Chem. Soc.* **2007**, *129*, 12676.

- [26] J. J. P. Kramer, M. Nieger, S. Brase, *Eur. J. Org. Chem.* **2013**, 541.
- [27] U. Wörsdörfer, F. Vögtle, M. Nieger, M. Waletzke, S. Grimme, F. Glorius, A. Pfaltz, *Synthesis* **1999**, 597.
- [28] J. Bruhin, W. Jenny, *Chimia* **1972**, 26, 420.
- [29] J. Bruhin, W. Jenny, *Tetrahedron Lett.* **1973**, 14, 1215.
- [30] T. Itoh, T. Iwasaki, M. Kubo, S. Iwatsuki, *Polym. Bull.* **1995**, 35, 307.
- [31] D. A. Black, R. E. Beveridge, B. A. Arndtsen, *J. Org. Chem.* **2008**, 73, 1906.
- [32] Z. Sun, S. Yu, Z. Ding, D. Ma, *J. Am. Chem. Soc.* **2007**, 129, 9300.
- [33] S. Yamada, A. Toshimitsu, Y. Takahashi, *Tetrahedron* **2009**, 65, 2329.
- [34] R. E. Beveridge, B. A. Arndtsen, *Synthesis* **2010**, 1000.
- [35] X. Jiang, H. Y. Chen, G. Galvan, M. Yoshida, J. Lahann, *Adv. Funct. Mater.* **2008**, 18, 27.
- [36] M. S. Kim, Y. N. Shin, M. H. Cho, S. H. Kim, S. K. Kim, Y. H. Cho, G. Khang, I. W. Lee, H. B. Lee, *Tissue Eng.* **2007**, 13, 2095.
- [37] T. Okano, N. Yamada, M. Okuhara, H. Sakai, Y. Sakurai, *Biomaterials* **1995**, 16, 297.
- [38] P. B. van Wachem, T. Beugeling, J. Feijen, A. Bantjes, J. P. Detmers, W. G. van Aken, *Biomaterials* **1985**, 6, 403.
- [39] J. H. Lee, J. W. Lee, G. Khang, H. B. Lee, *Biomaterials* **1997**, 18, 351.
- [40] H. Y. Chen, J. Lahann, *Adv. Mater.* **2007**, 19, 3801.
- [41] L. Bondarenko, I. Dix, H. Hinrichs, H. Hopf, *Synthesis* **2004**, 2751.
- [42] K. L. Parry, A. G. Shard, R. D. Short, R. G. White, J. D. Whittle, A. Wright, *Surf. Interface Anal.* **2006**, 38, 1497.
- [43] J. H. Scofield, *J. Electron Spectrosc. Relat. Phenom.* **1976**, 8, 129.
- [44] J. Lahann, I. S. Choi, J. Lee, K. F. Jensen, R. Langer, *Angew. Chem. Int. Ed.* **2001**, 40, 3166; *Angew. Chem.* **2001**, 113, 3273.
- [45] G. Sheldrick, *Acta Crystallogr. Sect. A* **2008**, 64, 112.
- [46] H. Flack, *Acta Crystallogr. Sect. A* **1983**, 39, 876.
- [47] R. W. W. Hoofstede, L. H. Straver, A. L. Spek, *J. Appl. Crystallogr.* **2008**, 41, 96.

Manuscript received: February 27, 2017

Accepted manuscript online: June 23, 2017

Version of record online: August 16, 2017